

# New high-statistics measurement of the $\pi^0 \rightarrow e^+e^-\gamma$ Dalitz decay at the Mainz Microtron

S. Prakhov,<sup>1,\*</sup> L. Heijkenskjöld,<sup>1</sup> S. Abt,<sup>2</sup> P. Achenbach,<sup>1</sup> P. Adlarson,<sup>1</sup> F. Afzal,<sup>3</sup> Z. Ahmed,<sup>4</sup> K. Altangerel,<sup>1</sup> J. R. M. Annand,<sup>5</sup> M. Bashkanov,<sup>6</sup> R. Beck,<sup>3</sup> M. Biroth,<sup>1</sup> N. S. Borisov,<sup>7,†</sup> A. Braghieri,<sup>8</sup> W. J. Briscoe,<sup>9</sup> F. Cividini,<sup>1</sup> C. Collicott,<sup>1</sup> S. Costanza,<sup>8</sup> A. Denig,<sup>1</sup> M. Dieterle,<sup>2</sup> A. S. Dolzhikov,<sup>7</sup> E. J. Downie,<sup>9</sup> P. Drexler,<sup>1</sup> S. Fegan,<sup>6</sup> S. Gardner,<sup>5</sup> D. Ghosal,<sup>2</sup> D. I. Glazier,<sup>5</sup> I. Gorodnov,<sup>7</sup> W. Grädl,<sup>1</sup> M. Günther,<sup>2</sup> G. M. Gurevich,<sup>10</sup> D. Hornidge,<sup>11</sup> G. M. Huber,<sup>4</sup> A. Käser,<sup>2</sup> V. L. Kashevarov,<sup>1,7</sup> S. J. D. Kay,<sup>4</sup> M. Korolija,<sup>12</sup> B. Krusche,<sup>2,†</sup> A. Lazarev,<sup>7</sup> K. Livingston,<sup>5</sup> S. Lutterer,<sup>2</sup> I. J. D. MacGregor,<sup>5</sup> D. M. Manley,<sup>13</sup> P. P. Martel,<sup>1</sup> R. Miskimen,<sup>14</sup> M. Mocanu,<sup>6</sup> E. Mornacchi,<sup>1</sup> C. Mullen,<sup>5</sup> A. Neganov,<sup>7</sup> A. Neiser,<sup>1</sup> M. Ostrick,<sup>1</sup> P. B. Otte,<sup>1</sup> D. Paudyal,<sup>4</sup> P. Pedroni,<sup>8</sup> A. Powell,<sup>5</sup> E. Rickert,<sup>1</sup> T. Rostomyan,<sup>2</sup> V. Sokhoyan,<sup>1</sup> K. Spieker,<sup>3</sup> O. Steffen,<sup>1</sup> I. I. Strakovsky,<sup>9</sup> Th. Strub,<sup>2</sup> I. Supek,<sup>12</sup> M. Thiel,<sup>1</sup> A. Thomas,<sup>1</sup> Yu. A. Usov,<sup>7</sup> S. Wagner,<sup>1</sup> D. P. Watts,<sup>6</sup> D. Werthmüller,<sup>6</sup> J. Wettig,<sup>1</sup> M. Wolfes,<sup>1</sup> and N. Zachariou<sup>6</sup>

(A2 Collaboration at MAMI)

<sup>1</sup>*Institut für Kernphysik, University of Mainz, D-55099 Mainz, Germany*

<sup>2</sup>*Institut für Physik, University of Basel, CH-4056 Basel, Switzerland*

<sup>3</sup>*Helmholtz-Institut für Strahlen- und Kernphysik, University of Bonn, D-53115 Bonn, Germany*

<sup>4</sup>*University of Regina, Regina, Saskatchewan S4S 0A2, Canada*

<sup>5</sup>*SUPA School of Physics and Astronomy, University of Glasgow, Glasgow G12 8QQ, United Kingdom*

<sup>6</sup>*Department of Physics, University of York, Heslington, York, Y010 5DD, United Kingdom*

<sup>7</sup>*Joint Institute for Nuclear Research, 141980 Dubna, Russia*

<sup>8</sup>*INFN Sezione di Pavia, I-27100 Pavia, Italy*

<sup>9</sup>*The George Washington University, Washington, DC 20052-0001, USA*

<sup>10</sup>*Institute for Nuclear Research, 125047 Moscow, Russia*

<sup>11</sup>*Mount Allison University, Sackville, New Brunswick E4L 1E6, Canada*

<sup>12</sup>*Rudjer Boskovic Institute, HR-10000 Zagreb, Croatia*

<sup>13</sup>*Kent State University, Kent, Ohio 44242-0001, USA*

<sup>14</sup>*University of Massachusetts, Amherst, Massachusetts 01003, USA*

(Dated: December 4, 2025)

The Dalitz decay  $\pi^0 \rightarrow e^+e^-\gamma$  has been measured with the highest statistical accuracy obtained so far in the  $\gamma p \rightarrow \pi^0 p$  reaction with the A2 tagged-photon facility at the Mainz Microtron, MAMI. The value of the slope parameter for the  $\pi^0$  electromagnetic transition form factor,  $a_\pi = 0.0315 \pm 0.0026_{\text{stat}} \pm 0.0010_{\text{syst}}$ , is obtained from the analysis of  $2.4 \times 10^6 \pi^0 \rightarrow e^+e^-\gamma$  observed decays. Within experimental uncertainties, it is in agreement with existing measurements and theoretical calculations, with its own uncertainty being smaller than previous results based on the analysis of  $\pi^0 \rightarrow e^+e^-\gamma$  decays.

## I. INTRODUCTION

The importance of measuring electromagnetic (e/m) transition form factors (TFFs) of light mesons, and especially  $\pi^0$ , for better understanding their properties and providing low-energy precision tests of the Standard Model (SM) and Quantum Chromodynamics (QCD), has been discussed in some detail in Ref. [1] dedicated to the previous A2 measurement of the  $\pi^0 \rightarrow e^+e^-\gamma$  Dalitz decay. In particular, for data-driven theoretical determinations of the anomalous magnetic moment of the muon ( $g-2)_\mu$  within the SM [2–4], the TFFs of light mesons enter as important contributions to the hadronic light-by-light (HLbL) scattering calculations [5–30]. If the TFF parameters are extracted from the  $\pi^0 \rightarrow e^+e^-\gamma$  Dalitz decay with a sufficient accuracy, they could then

constrain calculations that estimate the pion-pole term  $a_\mu^{\pi^0}$  to the HLbL scattering contribution to  $(g-2)_\mu$ , as well as the  $\pi^0\gamma$ -channel contribution  $a_\mu^{\pi^0\gamma}$  [31–36] to the hadronic-vacuum-polarization (HVP) correction [37, 38] to  $(g-2)_\mu$ .

For a structureless (point-like) meson  $A$ , its decays into a lepton pair plus a photon,  $A \rightarrow l^+l^-\gamma$ , can be described within Quantum Electrodynamics (QED) via  $A \rightarrow \gamma^*\gamma$ , with the virtual photon  $\gamma^*$  decaying into the lepton pair [39]. For the meson  $A$ , QED predicts a specific strong dependence of its decay rate on the dilepton invariant mass,  $m_{ll}^2 = q^2$ . A deviation from the pure QED dependence, caused by the actual electromagnetic structure of the meson  $A$ , is formally described by its e/m TFF [40]. The Vector-Meson-Dominance (VMD) model [41] can be used to describe the coupling of the virtual photon  $\gamma^*$  to the meson  $A$  via an intermediate virtual vector meson  $V$ . This mechanism is especially strong in the time-like (energy transfer larger than the momentum transfer) momentum-transfer region,  $(2m_l)^2 < q^2 < m_A^2$ , where a resonant behavior near  $q^2 = m_V^2$  of the vir-

\*corresponding author, e-mail: prakhov@ucla.edu

†deceased

tual photon arises because the virtual vector meson is approaching the mass shell [40]. Experimentally, time-like TFFs can be determined via measuring the differential decay width of  $A \rightarrow l^+l^-\gamma$  as a function of the dilepton invariant mass  $m_{ll}$ , normalizing this dependence to the partial decay width  $\Gamma(A \rightarrow \gamma\gamma)$ , and taking into account the pure QED dependence expected for the  $A \rightarrow \gamma^*\gamma \rightarrow l^+l^-\gamma$  differential decay width. Correspondingly, the  $\pi^0 \rightarrow \gamma^*\gamma \rightarrow e^+e^-\gamma$  differential decay width can be parametrized in the time-like region as [40]

$$\begin{aligned} \frac{d\Gamma(\pi^0 \rightarrow e^+e^-\gamma)}{dm_{ee}\Gamma(\pi^0 \rightarrow \gamma\gamma)} &= [\text{QED}(m_{ee})]|F_{\pi^0\gamma}(m_{ee})|^2 = \\ &= \frac{4\alpha}{3\pi m_{ee}} \times \left(1 - \frac{4m_e^2}{m_{ee}^2}\right)^{\frac{1}{2}} \left(1 + \frac{2m_e^2}{m_{ee}^2}\right) \left(1 - \frac{m_{ee}^2}{m_{\pi^0}^2}\right)^3 \times \\ &\times |F_{\pi^0\gamma}(m_{ee})|^2, \end{aligned} \quad (1)$$

where  $F_{\pi^0\gamma}$  is the normalized TFF of the  $\pi^0$  meson,  $m_{\pi^0}$  and  $m_e$  are the masses of the  $\pi^0$  meson and  $e^\pm$ , respectively. Because of the smallness of the momentum-transfer range for the  $\pi^0 \rightarrow e^+e^-\gamma$  decay, its normalized TFF is typically parametrized as [42]

$$F_{\pi^0\gamma}(m_{ee}) = 1 + a_\pi \frac{m_{ee}^2}{m_{\pi^0}^2}, \quad (2)$$

where the parameter  $a_\pi$  reflects the TFF slope at  $m_{ee}^2 = 0$ . A simple VMD model incorporates only the  $\rho$ ,  $\omega$ , and  $\phi$  resonances (in the narrow-width approximation) as virtual vector mesons driving the photon interaction in  $A \rightarrow \gamma^*\gamma$ . Using a quark model for the corresponding couplings leads to neglecting  $\phi$  and yields [40]  $a_\pi/m_{\pi^0}^2 = 0.5(1 + m_\rho^2/m_\omega^2)/m_\rho^2 \approx 1.648 \text{ GeV}^{-2}$  (or  $a_\pi \approx 0.0300$ ) for the  $\pi^0$  Dalitz decay.

Another feature of the  $\pi^0 \rightarrow e^+e^-\gamma$  decay amplitude is an angular anisotropy of the virtual photon decaying into the  $e^+$ ,  $e^-$ , and  $\gamma$  in the  $\pi^0$  rest frame, the angle  $\theta_e$  between the direction of one of the leptons in the virtual-photon (or dilepton) rest frame and the direction of the dilepton system (which is opposite to the  $\gamma$  direction) follows the dependence [43]

$$f(\cos \theta_e) = 1 + \cos^2 \theta_e + \left(\frac{2m_e}{m_{ee}}\right)^2 \sin^2 \theta_e, \quad (3)$$

with the  $\sin^2 \theta_e$  term becoming very small when  $m_{ee} \gg 2m_e$ . Both the  $[\text{QED}(m_{ee})]$  term in Eq.(1) and the angular dependence in Eq.(3) represent only the leading-order term of the  $\pi^0 \rightarrow e^+e^-\gamma$  decay amplitude, and radiative corrections need to be considered for a more accurate calculation of  $[\text{QED}(m_{ee}, \cos \theta_e)]$ . The introduction of radiative corrections modifies Eq.(1) as

$$\frac{d\Gamma(\pi^0 \rightarrow e^+e^-\gamma)}{dm_{ee}\Gamma(\pi^0 \rightarrow \gamma\gamma)} = [\text{QED}(m_{ee})](1 + \delta(m_{ee}))|F_{\pi^0\gamma}(m_{ee})|^2, \quad (4)$$

where  $\delta(m_{ee})$  is radiative correction as a function of  $m_{ee}$  integrated over the full  $\cos \theta_e$  range. The most recent calculations of radiative corrections to the differential

decay rate of the Dalitz decay  $\pi^0 \rightarrow e^+e^-\gamma$  were reported in Ref. [44]. In this work, the radiative corrections derived by Mikaelian and Smith [45] to the leading-order (LO) differential decay rate of the Dalitz decay  $\pi^0 \rightarrow e^+e^-\gamma$  were recalculated beyond the soft-photon approximation. The next-to-leading-order (NLO) corrections were divided into three parts emphasizing their origin. They included the virtual radiative corrections coming from both the electron and muon loops, the one-photon-irreducible contribution at one-loop level, and the bremsstrahlung correction.

The first high-statistics measurements of the time-like  $\pi^0$  TFF were conducted somewhat recently by the A2 [1] and NA62 [46] Collaborations via the analysis of  $0.4 \times 10^6$  and  $1.1 \times 10^6$  Dalitz decays  $\pi^0 \rightarrow e^+e^-\gamma$ , respectively. Before that, the magnitude of the Dalitz-decay slope parameter  $a_\pi$  and its uncertainty in the Review of Particle Physics (RPP) from 2014 [47],  $a_\pi = 0.032 \pm 0.004$ , were mostly determined by a measurement of the space-like  $\pi^0$  TFF in the process  $e^+e^- \rightarrow e^+e^-\pi^0$  by the CELLO detector [48]. Adding the A2 value  $a_\pi = 0.030 \pm 0.010_{\text{tot}}$  [1] and  $a_\pi = 0.0368 \pm 0.0051_{\text{stat}} \pm 0.0025_{\text{syst}} = 0.0368 \pm 0.0057_{\text{tot}}$  from the NA62 [46] measurement [46] in the RPP average resulted in its new value  $a_\pi = 0.0332 \pm 0.0029$  [42], which is slightly larger than the previous RPP value, mostly due to smaller uncertainties in the NA62 result.

Quite recent theoretical calculations for the  $\pi^0 \rightarrow \gamma^*\gamma \rightarrow e^+e^-\gamma$  TFF, in addition to the slope parameter  $a_\pi$ , also involve the curvature parameter  $b_\pi$ :

$$F_{\pi^0\gamma}(m_{ee}) = 1 + a_\pi \frac{m_{ee}^2}{m_{\pi^0}^2} + b_\pi \frac{m_{ee}^4}{m_{\pi^0}^4}. \quad (5)$$

A calculation based on a model-independent method using Padé approximants was reported in Ref. [49]. The analysis of space-like data (CELLO [48], CLEO [50], BABAR [51], and Belle [52]) with this method provides a good and systematic description of the low-energy region, resulting in  $a_\pi = 0.0324 \pm 0.0012_{\text{stat}} \pm 0.0019_{\text{syst}}$  and  $b_\pi = (1.06 \pm 0.09_{\text{stat}} \pm 0.25_{\text{syst}}) \cdot 10^{-3}$ . Adding the latest time-like data in this method will definitely constrain these calculations to a better accuracy. Values with even smaller uncertainties,  $a_\pi = 0.0307 \pm 0.0006$  and  $b_\pi = (1.10 \pm 0.02) \cdot 10^{-3}$ , were obtained by using dispersion theory [53]. In that analysis, the singly virtual TFF was calculated in both the time-like and the space-like regions, based on data for the  $e^+e^- \rightarrow 3\pi$  cross section, generalizing previous studies on  $\omega/\phi \rightarrow 3\pi$  decays [54] and  $\gamma\pi \rightarrow \pi\pi$  scattering [55], and verifying the results by comparing them to time-like  $e^+e^- \rightarrow \pi^0\gamma$  data at larger momentum transfer. This analysis was later revised to match better the high-energy asymptotics that become more relevant once the TFF is incorporated into the HLbL loop integral for the  $(g-2)_\mu$  contribution, which resulted in the new value  $a_\pi = 0.0315 \pm 0.0009$  [9, 10].

In this paper, a new high-statistics measurement of the  $\pi^0 \rightarrow e^+e^-\gamma$  Dalitz decay with the A2 experimental setup at MAMI is reported. The experiment was conducted in 2018 by producing  $\sim 3.31 \times 10^9 \pi^0$  mesons in

the reaction  $\gamma p \rightarrow \pi^0 p$ , which made it possible to accumulate  $\sim 2.3 \times 10^6$   $\pi^0 \rightarrow e^+ e^- \gamma$  decays available for the experimental analysis, compared to  $\sim 0.4 \cdot 10^6$  decays used in the previous measurement by the A2 Collaboration [1]. The  $\pi^0$  TFF parameters and their uncertainties extracted in the present measurement represent a further and more accurate experiment in the time-like momentum-transfer region that aims to better constrain calculations estimating  $(g - 2)_\mu$  contributions from the pion-pole term  $a_\mu^{\pi^0}$  to the HLB scattering and the  $\pi^0 \gamma$  term  $a_\mu^{\pi^0 \gamma}$  to the HVP correction.

## II. EXPERIMENTAL SETUP

The process  $\gamma p \rightarrow \pi^0 p \rightarrow e^+ e^- \gamma p$  was measured at the the Mainz Microtron (MAMI) [56, 57], using an energy-tagged bremsstrahlung photon beam. The energies of the incident photons were analyzed up to 750 MeV, by detecting the post-bremsstrahlung electrons in the Glasgow–Mainz tagged-photon spectrometer (Tagger) [58], detectors and electronics of which underwent a major upgrade in 2017 [59]. The uncertainty of  $\pm 1.5$  MeV in the energy of the tagged photons was mostly determined by the segmentation of the focal-plane detector of the Tagger in combination with the energy of the MAMI electron beam, which was set for the present experiment at 883 MeV.

The final-state particles produced in the  $\gamma p$  interactions were detected by using the Crystal Ball (CB) [60] as a central calorimeter and TAPS [61, 62] as a forward calorimeter. The CB detector consists of 672 NaI(Tl) crystals covering polar angles from  $20^\circ$  to  $150^\circ$ . The TAPS calorimeter consists of 366 BaF<sub>2</sub> crystals covering polar angles from  $4^\circ$  to  $20^\circ$  and 72 PbWO<sub>4</sub> crystals with angular coverage from  $1^\circ$  to  $4^\circ$ . Both the CB and TAPS calorimeters have full azimuthal coverage. More information regarding the energy and angular resolution of the CB and TAPS detectors is provided in Refs. [63, 64].

Linear-polarized photons, produced by coherent bremsstrahlung of the MAMI beam electrons in a 100- $\mu\text{m}$ -thick diamond radiator and collimated by a 3-mm-diameter Pb collimator, were incident on a 10-cm-long liquid hydrogen (LH<sub>2</sub>) target located in the center of the CB. The coherent peak was positioned at the center-of-mass energy corresponding to the maximum of the  $\Delta(1232)$  resonance, enhancing significantly pion photo-production. The total amount of material around the LH<sub>2</sub> target, including the Kapton cell and the 1-mm-thick carbon-fiber beamline, was equivalent to 0.8% of a radiation length  $X_0$ . In the present measurement, it was essential to keep the material budget as low as possible to minimize the background from  $\pi^0 \rightarrow \gamma\gamma$  decays with conversion of the photons into  $e^+ e^-$  pairs. The LH<sub>2</sub> target was surrounded by a Particle IDentification (PID) detector [66] used to distinguish between charged and neutral particles. It was made of 24 scintillator bars (50 cm long, 4 mm thick) arranged as a cylinder with a radius of 12 cm. The experimental trigger required the total energy

deposited in the CB to exceed  $\sim 140$  MeV.

## III. DATA HANDLING

### A. Event selection

To search for a signal from  $\pi^0 \rightarrow e^+ e^- \gamma$  decays, candidates for the process  $\gamma p \rightarrow e^+ e^- \gamma p$  were extracted from events having three or four clusters reconstructed by a software analysis in the CB and TAPS together. The procedure used in the present analysis for the event selection was quite similar to the previous A2 measurement of this decay reported in Ref. [1]. The offline cluster algorithm was optimized for finding a group of adjacent crystals in which the energy was deposited by a single-photon e/m shower. This algorithm works well for  $e^\pm$ , which also produce e/m showers in the CB and TAPS, and for proton clusters. The software threshold for the cluster energy was chosen to be 12 MeV. For the  $\gamma p \rightarrow e^+ e^- \gamma p$  candidates, the three-cluster events were analyzed assuming that the final-state proton was not detected.

The selection of candidate events and the reconstruction of the reaction kinematics were based on the kinematic-fit technique. Details of the kinematic-fit parametrization of the detector information and resolutions are given in Ref. [63]. Because e/m showers from electrons and positrons are very similar to those of photons, the hypothesis  $\gamma p \rightarrow 3\gamma p$  was tested to identify the  $\gamma p \rightarrow e^+ e^- \gamma p$  candidates. The events that satisfied this hypothesis with the probability (or confidence level, CL) greater than 1% were accepted for further analysis. The kinematic-fit output was used to reconstruct the kinematics of the outgoing particles. In this output, there was no separation between e/m showers caused by the outgoing photon, electron, or positron. In the further analysis the separation of  $e^+ e^-$  pairs from final-state photons was based on the information from the PID detector. This procedure was optimized by using a Monte Carlo (MC) simulation of the signal events and the main background reactions.

To minimize systematic uncertainties in the determination of experimental acceptances and to measure the TFF energy dependence properly, the MC simulation of the signal events was made to be as close as possible to the behavior of real  $\gamma p \rightarrow \pi^0 p \rightarrow e^+ e^- \gamma p$  events. To reproduce the experimental yield of  $\pi^0$  mesons and their center-of-mass angular distributions as a function of the incident-photon energy, the  $\gamma p \rightarrow \pi^0 p \rightarrow \gamma\gamma p$  reaction was measured in the same experiment for every individual Tagger channel by using the  $\pi^0 \rightarrow \gamma\gamma$  decay and then used as an input in the MC event generator. The results obtained here for the  $\pi^0$  photoproduction angular distributions in the center-of-mass frame at the energies of each Tagger channel were in good agreement with the previous A2 results for the differential cross sections of  $\pi^0$  photoproduction on the free proton [67, 68].

The  $\pi^0 \rightarrow e^+ e^- \gamma$  decays were generated according to Eq.(1), with the phase-space term removed and with

the slope parameter of the  $\pi^0$  electromagnetic transition form factor from Eq.(2) taken as  $a_\pi = 0.032$ , which is close to the value expected from the theoretical calculations [9, 10, 49]. Such a value slightly increase the population of MC events at large  $m(e^+e^-)$  masses, which are needed for the acceptance determination, but does not affect its value extracted from the analysis of the corresponding MC simulations. The angular dependence of the virtual photon decaying into the  $e^+e^-$  pair was generated according to Eq.(3). These dependences from the leading-order QED term of the decay amplitude were then convoluted with radiative corrections based on the calculations of Ref. [44]. The event vertices were generated uniformly along the 10-cm length of the LH<sub>2</sub> target. Similarly to the  $\gamma p \rightarrow \pi^0 p \rightarrow e^+e^-\gamma p$  process, the MC generator for the main background process  $\gamma p \rightarrow \pi^0 p \rightarrow \gamma\gamma p$  used the experimental spectra measured in the same experiment.

For both  $\pi^0$  decay modes, the generated events were propagated through a GEANT (version 3.21) simulation of the experimental setup. To reproduce the resolutions observed in the experimental data, the GEANT output (energy and timing) was subject to additional smearing, thus allowing both the simulated and experimental data to be analyzed in the same way. Matching the energy resolution between the experimental and MC events was achieved by adjusting the invariant-mass resolutions, the kinematic-fit stretch functions (or pulls), and probability distributions. Such an adjustment was based on the analysis of the same data sets for the reaction  $\gamma p \rightarrow \pi^0 p \rightarrow \gamma\gamma p$ , having almost no background from other physical reactions at these energies. The simulated events were also tested to check whether they passed the trigger requirements.

The PID detector was used to identify the final-state  $e^+e^-$  pair in the events initially selected as  $\gamma p \rightarrow 3\gamma p$  candidates. Only events with three e/m showers in the CB were selected for further analysis because the PID provides full coverage of the LH<sub>2</sub> target solely for the CB. The identification of  $e^\pm$  in the CB was based on a correlation between azimuthal angles of fired PID elements with the corresponding angles of e/m showers in the calorimeter. The MC simulations of  $\gamma p \rightarrow \pi^0 p \rightarrow e^+e^-\gamma p$  and  $\gamma p \rightarrow \pi^0 p \rightarrow \gamma\gamma p$  were used to optimize this procedure, minimizing the probability for misidentifying  $e^\pm$  with the final-state photons and protons and suppressing the major background process.

The MC simulation for the main background reaction  $\gamma p \rightarrow \pi^0 p \rightarrow \gamma\gamma p$  demonstrated that this process can mimic  $\pi^0 \rightarrow e^+e^-\gamma$  events when one of the final-state photons is converted into an  $e^+e^-$  pair in the material between the production vertex and the NaI(Tl) surface. The reconstructed  $m(e^+e^-\gamma)$  distribution for such a background is typically peaked near the  $\pi^0$  mass. Because the opening angle between the conversion electron and positron is typically very small, this background contributes mostly to low invariant masses  $m(e^+e^-)$ . Requiring  $e^+$  and  $e^-$  to be identified by different PID elements suppresses this background significantly. Such a

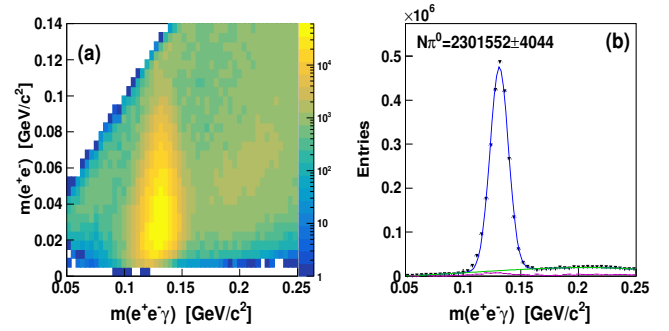


FIG. 1: (Color online) Experimental events selected as  $\gamma p \rightarrow e^+e^-\gamma p$  candidates by requiring the kinematic-fit  $CL(\gamma p \rightarrow 3\gamma p) > 1\%$  and  $e^\pm$  to be identified by using  $dE/dx$  from the PID to suppress their misidentification with recoiling protons: (a) the two-dimensional distribution of  $m(e^+e^-\gamma)$  vs  $m(e^+e^-)$ ; (b) the  $m(e^+e^-\gamma)$  distribution fitted with the sum of a Gaussian for the  $\pi^0 \rightarrow e^+e^-\gamma$  peak (blue line) and a polynomial of order 4 for the background (green line), and the subtracted empty-target background shown by the magenta line.

requirement also results in losses of actual  $\pi^0 \rightarrow e^+e^-\gamma$  events. However, it mostly affects low invariant masses  $m(e^+e^-)$ , which are less important for measuring the TFF slope parameter.

For both the  $\gamma p \rightarrow \pi^0 p \rightarrow e^+e^-\gamma p$  and  $\gamma p \rightarrow \pi^0 p \rightarrow \gamma\gamma p$  reactions, there is a chance that the recoil proton is misidentified as  $e^\pm$ . Such a background does not mimic the  $\pi^0$  peak in the  $m(e^+e^-\gamma)$  spectrum, but its suppression improves the signal-to-background ratio, which is important for more reliable fitting of the signal peak above the remaining background. The background from the misidentification of the recoil proton with  $e^\pm$  can be suppressed by the analysis of energy losses,  $dE/dx$ , in the PID elements. To reflect the actual differential energy deposit  $dE/dx$  in the PID, the energy signal from each element, ascribed to either  $e^+$  or  $e^-$ , was multiplied by the sine of the polar angle of the corresponding particle, the magnitude of which was taken from the kinematic-fit output. All PID elements were calibrated so that the  $e^\pm$  peak position matched the corresponding peak in the MC simulation. To reproduce the actual energy resolution of the PID with the MC simulation, the GEANT output for PID energies was subject to additional smearing, allowing the  $e^\pm$  selection with  $dE/dx$  cuts to be very similar for the experimental and MC simulated data. The PID energy resolution in the MC simulations was adjusted to match the experimental  $dE/dx$  spectra for the  $e^\pm$  particles from  $\pi^0 \rightarrow e^+e^-\gamma$  decays observed experimentally. Possible systematic uncertainties due to the  $dE/dx$  cuts were checked via the stability of the results after narrowing the  $dE/dx$  range for selecting  $e^\pm$ . Additional information on using the  $dE/dx$  PID for event selection and the agreement between the experimental data and MC simulations can be found in Ref. [1].

In addition to the background contributions discussed above, there are two more of those that can be subtracted

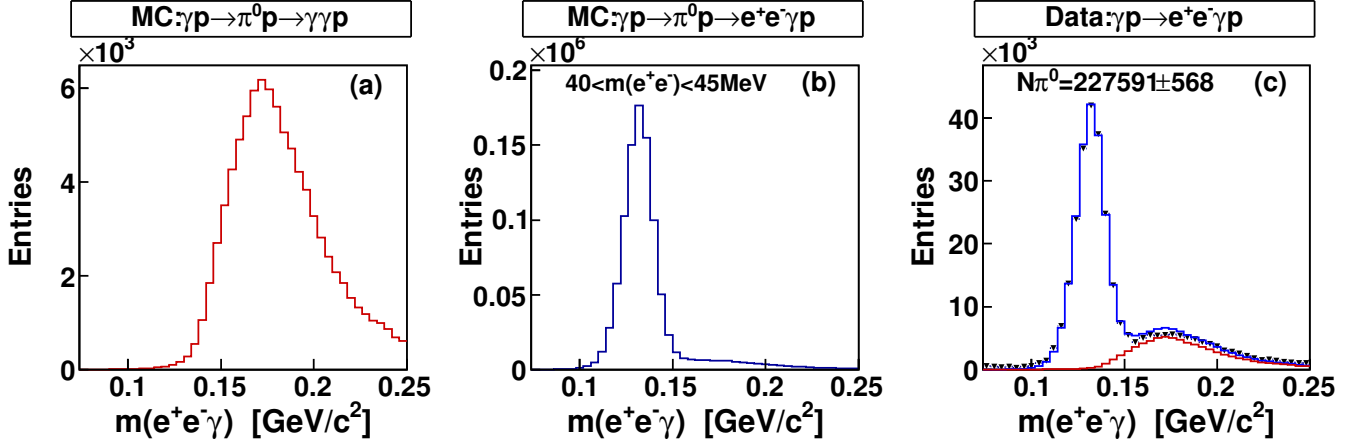


FIG. 2: (Color online)  $m(e^+e^-\gamma)$  invariant-mass distributions obtained in the range  $40 < m(e^+e^-) < 45$  MeV/ $c^2$  with  $\gamma p \rightarrow e^+e^-\gamma p$  candidates selected without using a  $dE/dx$  PID cut to separate  $e^\pm$  from the recoil protons: (a) MC simulation of  $6.2 \times 10^9 \gamma p \rightarrow \pi^0 p \rightarrow \gamma\gamma p$  events; (b) MC simulation of  $1.6 \times 10^8 \gamma p \rightarrow \pi^0 p \rightarrow e^+e^-\gamma p$  events; (c) experimental spectrum (solid triangles with error bars) fitted with the sum of the  $\gamma p \rightarrow \pi^0 p \rightarrow e^+e^-\gamma p$  and  $\gamma p \rightarrow \pi^0 p \rightarrow \gamma\gamma p$  MC simulations (shown by the blue line), with the fraction of the  $\gamma p \rightarrow \pi^0 p \rightarrow \gamma\gamma p$  background shown by the red line.

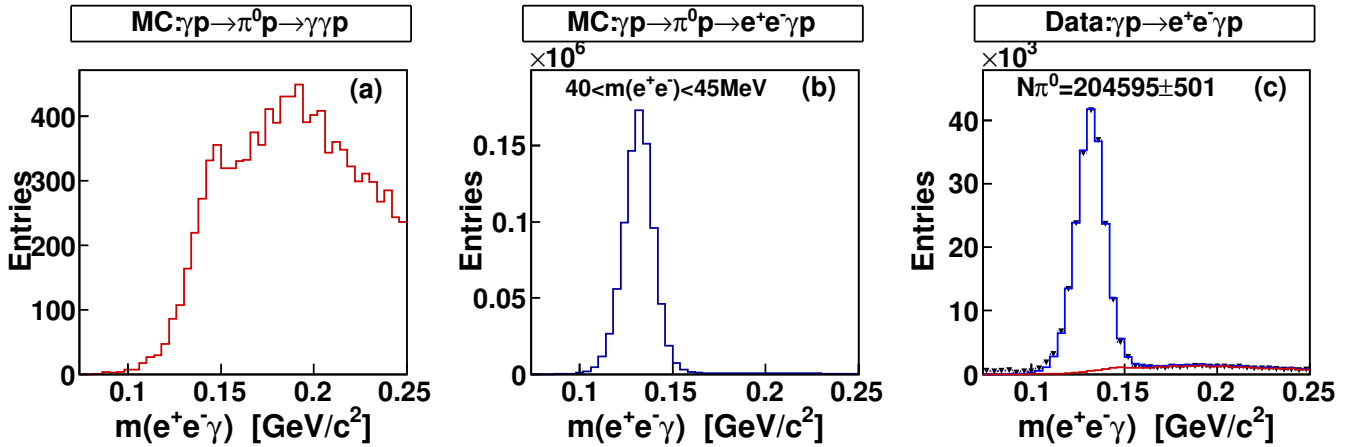


FIG. 3: (Color online) Same as Fig. 2, but with the use of a  $dE/dx$  PID cut to separate  $e^\pm$  from the recoil protons.

directly in the data analysis. The first contribution comes from interactions of incident photons in the windows of the target cell. The subtraction of this background was based on the analysis of data samples that were taken with an empty target. The weight for the subtraction of the empty-target spectra was taken as a ratio of the photon-beam fluxes for the data samples with the full and the empty target. Another background was caused by random coincidences of the Tagger counts with the experimental trigger; its subtraction was carried out by using event samples for which all coincidences were random (see Refs. [63, 64] for more details).

### B. Analysis of $\pi^0 \rightarrow e^+e^-\gamma$ decays

The two-dimensional distribution of  $m(e^+e^-\gamma)$  vs  $m(e^+e^-)$  is shown in Fig. 1(a) for all selected experimental events after subtracting the empty-target and random

backgrounds and suppressing the misidentification of the recoil protons with  $e^\pm$  by the  $dE/dx$  PID cuts. The actual  $\pi^0 \rightarrow e^+e^-\gamma$  decays are seen there as a vertical band along  $m(e^+e^-\gamma)$  with its invariant-mass spectrum peaking at the  $\pi^0$  mass. The corresponding  $m(e^+e^-\gamma)$  projection is shown in Fig. 1(b). To estimate the number of  $\pi^0 \rightarrow e^+e^-\gamma$  decays detected in the present experiment, the  $m(e^+e^-\gamma)$  distribution was fitted with the sum of a Gaussian for the  $\pi^0 \rightarrow e^+e^-\gamma$  peak (blue line) and a polynomial of order 4 for the background (green line). The subtracted empty-target background is shown in the same figure by a magenta line. Based on this fit, the total number of the detected  $\pi^0 \rightarrow e^+e^-\gamma$  decays is  $\sim 2.3 \times 10^6$ , which is significantly larger than any of those numbers observed in the previous measurements of this decay [1, 46]. The background under the  $\pi^0 \rightarrow e^+e^-\gamma$  peak nearly all comes from  $\pi^0 \rightarrow \gamma\gamma$  decays. Based on the number of  $\gamma p \rightarrow \pi^0 p \rightarrow \gamma\gamma p$  events observed in this experiment ( $3.27 \times 10^9$ ), the fraction of those events that

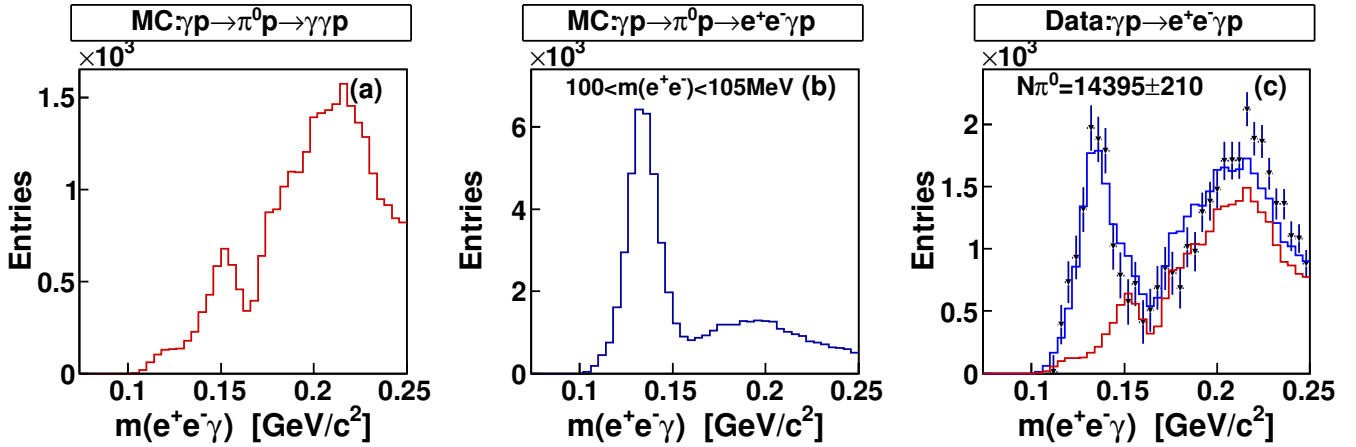


FIG. 4: (Color online) Same as Fig. 2, but for the invariant-mass range  $100 < m(e^+e^-) < 105$  MeV/c $^2$ .

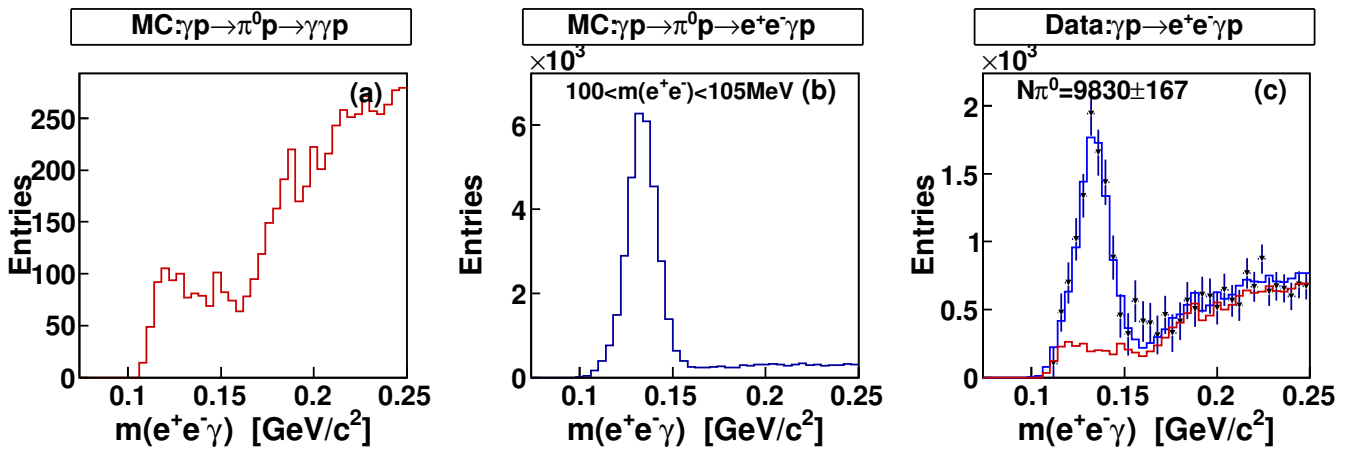


FIG. 5: (Color online) Same as Fig. 4, but with using a  $dE/dx$  PID cut to separate  $e^\pm$  from the recoil protons.

contributed to this background is only 0.02%.

To measure the  $\pi^0 \rightarrow e^+e^-\gamma$  yield as a function of the invariant mass  $m(e^+e^-)$ , the selected events were divided into 5-MeV-wide  $m(e^+e^-)$  bins. Events with  $m(e^+e^-) < 15$  MeV/c $^2$  were not analyzed because e/m showers from those  $e^+$  and  $e^-$  often overlap in the CB and hit the same PID element. The number of  $\pi^0 \rightarrow e^+e^-\gamma$  decays in every  $m(e^+e^-)$  bin was determined by fitting the  $m(e^+e^-\gamma)$  spectra obtained from the analysis of the MC simulations for the  $\pi^0 \rightarrow e^+e^-\gamma$  and  $\pi^0 \rightarrow \gamma\gamma$  decays to the corresponding experimental spectra by using the binned maximum-likelihood method. Such an approach helps to describe better the signal peak as well as the background shape from the events in which the recoil proton was misidentified with  $e^\pm$ .

The fitting procedure for measuring the number of reconstructed  $\pi^0 \rightarrow e^+e^-\gamma$  decays and the impact of applying a  $dE/dx$  PID cut on the fraction of background events is illustrated in Figs. 2–5 for two different  $m(e^+e^-)$  bins. Figure 2 shows the  $m(e^+e^-\gamma)$  invariant-mass spectra obtained for the MC simulations of  $\gamma p \rightarrow \pi^0 p \rightarrow \gamma\gamma p$  and  $\gamma p \rightarrow \pi^0 p \rightarrow e^+e^-\gamma p$  and their fit to the experimental distribution reconstructed in the range  $40 < m(e^+e^-) <$

45 MeV/c $^2$ . There was no  $dE/dx$  PID cut applied to obtain these spectra. Figure 3 illustrates the impact of the  $dE/dx$  PID cut on the fraction of background events in which the recoil proton was misidentified with  $e^\pm$ . As shown, applying the  $dE/dx$  PID cut reduces the background from  $\gamma p \rightarrow \pi^0 p \rightarrow \gamma\gamma p$  by more than one order of magnitude. For  $\gamma p \rightarrow \pi^0 p \rightarrow e^+e^-\gamma p$  events, the same cut practically eliminates all background under the  $\pi^0$  peak, with a quite small reduction of the  $\pi^0$  peak itself. The fit of the two MC simulations  $\gamma p \rightarrow \pi^0 p \rightarrow \gamma\gamma p$  and  $\gamma p \rightarrow \pi^0 p \rightarrow e^+e^-\gamma p$  to the experimental spectrum appears to be sufficient for its good description. The agreement observed between the experimental and MC peaks from  $\pi^0 \rightarrow e^+e^-\gamma$  decays confirms the agreement of the experimental data and the MC simulations in the energy calibration and resolution of the calorimeters. Figures 4 and 5 illustrate the fitting procedure of the  $m(e^+e^-\gamma)$  invariant-mass spectra in the range of high  $m(e^+e^-)$  masses, where the signal-to-background ratio drops significantly, again obtained before and after applying the  $dE/dx$  PID cut. As shown, applying the  $dE/dx$  PID cut in the range of high  $m(e^+e^-)$  masses still leaves a significant fraction of background events under the  $\pi^0$

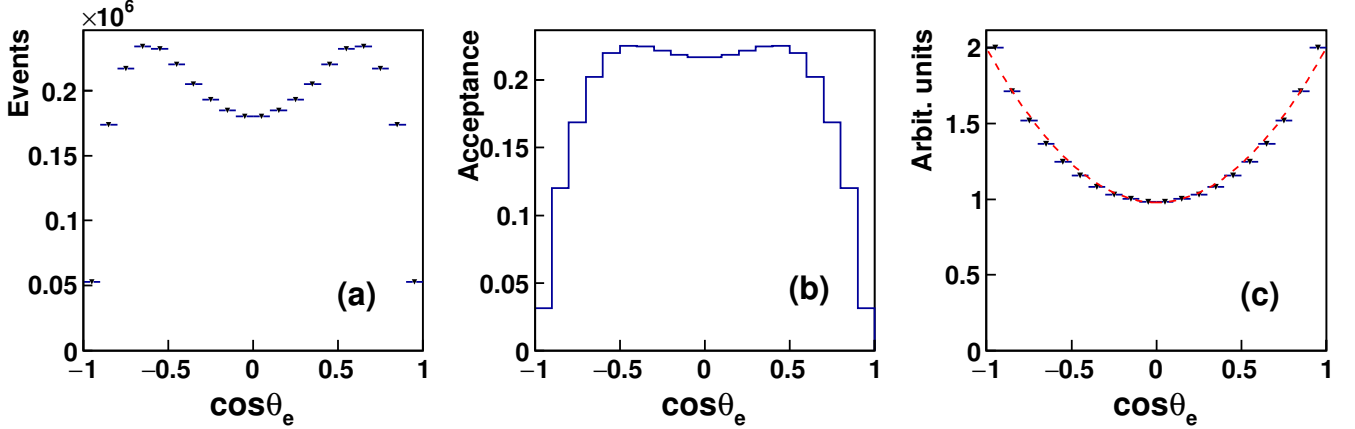


FIG. 6: (Color online) The  $\pi^0 \rightarrow \gamma\gamma^* \rightarrow \gamma e^+ e^-$  angular dependence (in the  $\pi^0$  rest frame) of the virtual photon decaying into a  $e^+ e^-$  pair, with  $\theta_e$  being the angle between the direction of one of the leptons in the virtual-photon (or the dilepton) rest frame and the direction of the dilepton system (which is opposite to the  $\gamma$  direction): (a) experimental events from the  $\pi^0 \rightarrow \gamma e^+ e^-$  peak; (b) angular acceptance based on the MC simulation; (c) the experimental spectrum corrected for the acceptance and normalized to the corresponding theoretical prediction (shown by a red dashed line). Because  $e^+$  and  $e^-$  cannot be separated in the present experiment, the angles of both leptons were used, resulting in a symmetric shape with respect to  $\cos \theta_e = 0$ .

peak.

The invariant-mass range  $15 < m(e^+ e^-) < 60$  MeV/ $c^2$ , which has the smallest fraction of background events under the  $\pi^0$  peak, was also used to measure the  $\pi^0 \rightarrow \gamma\gamma^* \rightarrow \gamma e^+ e^-$  angular dependence  $\cos \theta_e$  of the virtual photon decaying into an  $e^+ e^-$  pair and to compare it to the dependence determined by Eq.(3) folded with the corresponding radiative corrections [44]. The experimental results for such an angular dependence are illustrated in Fig. 6, which depicts the experimental distribution in Fig. 6(a), the angular acceptance determined from the MC simulation in Fig. 6(b), and the experimental distribution corrected for the acceptance and compared to the theoretical prediction in Fig. 6(c). As shown, in general there is good agreement between the measured and the predicted angular dependence. The very small difference between the reconstructed angular distribution and its theoretical prediction may be due to a small background contribution still remaining in the experimental data and/or due to smearing effects caused by the experimental angular resolution. Because  $e^+$  and  $e^-$  cannot be separated in the present experiment, the angles of both leptons were used to measure the angular dependence of the decaying dilepton, which resulted in a symmetric shape with respect to  $\cos \theta_e = 0$ .

#### IV. RESULTS AND DISCUSSION

The total number of  $\pi^0 \rightarrow e^+ e^- \gamma$  decays produced in each  $m(e^+ e^-)$  bin was obtained by correcting the number of decays observed in those bins with the corresponding detection efficiency. The detection efficiency itself depends strongly on the selection criteria applied. For the initial selection criteria, the detection efficiency rises from 7.06% at  $15 < m(e^+ e^-) < 20$  MeV/ $c^2$  to

25.9% at  $40 < m(e^+ e^-) < 45$  MeV/ $c^2$ . The results for  $|F_{\pi^0\gamma}(m_{e^+e^-})|^2$  were obtained from the numbers of  $\pi^0 \rightarrow e^+ e^- \gamma$  decays produced in each  $m(e^+ e^-)$  bin, taking into account the total number of  $\pi^0 \rightarrow \gamma\gamma$  decays produced in the same data and the  $[\text{QED}(m_{ee})]$  term from Eq.(4) after applying radiative corrections according to the calculations of Ref. [44]. The magnitude of radiative corrections as a two-dimensional function  $\delta(m_{ee}, \cos \theta_e)$  is depicted in Fig. 7. As shown, radiative corrections make the angular dependence of the virtual-photon decay weaker. For the  $\pi^0$  Dalitz decay, the corrected  $[\text{QED}(m_{ee})]$  term integrated over  $\cos \theta_e$  becomes  $\sim 1\%$  larger at  $m(e^+ e^-) = 15$  MeV, and  $\sim 10\%$  lower at  $m(e^+ e^-) = 120$  MeV. Such radiative corrections make the  $|F_{\pi^0\gamma}(m_{e^+e^-})|^2$  results at high  $m(e^+ e^-)$  masses very sensitive to the magnitude of those corrections and to a possible impact on it from next-to-next-to-leading-order (NNLO) terms, which were not taken into account in the calculations of Ref. [44]. It was also checked that the  $|F_{\pi^0\gamma}(m_{e^+e^-})|^2$  results do not follow directly the change in the magnitude of radiative corrections, because the experimental acceptance slightly improves when those corrections are applied, especially at high  $m(e^+ e^-)$  masses. Such an improvement is because fewer events are remaining at the extreme  $\theta_e$ , where the experimental acceptance drops (see Fig. 6(b)).

The uncertainty in an individual  $|F_{\pi^0\gamma}(m_{e^+e^-})|^2$  value from a particular fit was based on the uncertainty in the number of  $\pi^0 \rightarrow e^+ e^- \gamma$  decays determined by this fit. For each individual  $m(e^+ e^-)$  bin, the fitting procedure was repeated multiple times after refilling the  $m(e^+ e^- \gamma)$  spectra with different combinations of selection criteria, which were used to improve the signal-to-background ratio. The changes in selection criteria included different cuts on PID  $dE/dx$ , the kinematic-fit CL (such as 1%, 2%, 5%, and 10%), the incident-photon energy range

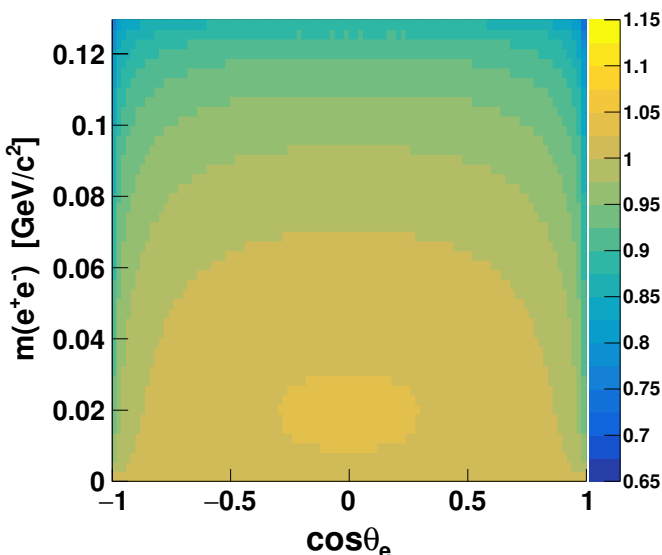


FIG. 7: (Color online) Magnitude of radiative corrections  $\delta(m_{ee}, \cos \theta_e)$  from Ref. [44] to the  $[\text{QED}(m_{ee}, \cos \theta_e)]$  term of Eq.(4).

(excluding higher energies with larger cross sections for the reactions  $\gamma p \rightarrow \pi^0 \pi^0 p$  and  $\gamma p \rightarrow \pi^0 \pi^+ n$ ). For a particular  $m(e^+e^-)$  bin, the fit result with the smallest  $\delta N(\pi^0 \rightarrow e^+e^-\gamma)/N(\pi^0 \rightarrow e^+e^-\gamma)$  was taken as the main result, in order to provide the smallest uncertainty in the slope parameter from fitting to the  $|F_{\pi^0\gamma}(m_{e^+e^-})|^2$  data points. The other results were used to evaluate the systematic uncertainty in the measured value for the slope parameter of the  $\pi^0$  e/m TFF. The magnitude of individual  $\delta N(\pi^0 \rightarrow e^+e^-\gamma)/N(\pi^0 \rightarrow e^+e^-\gamma)$  errors from fitting to the  $m(e^+e^-\gamma)$  invariant mass spectra was for the most part determined by the number of  $\pi^0 \rightarrow e^+e^-\gamma$  events in the peak and the background level under it.

In the previous measurement [1] by the A2 Collaboration, the main result for a particular  $m(e^+e^-)$  bin was obtained by averaging the results of all fits made for this bin, in a way that reduced the scattering of the measured  $|F_{\pi^0\gamma}(m_{e^+e^-})|^2$  values from one  $m(e^+e^-)$  bin to another. Then the uncertainty based on the smallest  $\delta N(\pi^0 \rightarrow e^+e^-\gamma)/N(\pi^0 \rightarrow e^+e^-\gamma)$  was added in quadrature with the systematic uncertainty calculated as the root mean square of the results from all fits made for this bin. However, such an approach turned out to be too conservative in the evaluation of the total uncertainties in the  $|F_{\pi^0\gamma}(m_{e^+e^-})|^2$  values for each individual  $m(e^+e^-)$  bin, as the magnitude of those total uncertainties looked significantly larger compared to the actual scattering of the data points. Moreover, the slope parameter obtained from fitting those  $|F_{\pi^0\gamma}(m_{e^+e^-})|^2$  data points did not provide a separation of the statistical and the systematic components in the total uncertainty for the slope parameter.

The  $|F_{\pi^0\gamma}(m_{e^+e^-})|^2$  data points from the present work are depicted in Fig. 8 along with the results of previous

measurements by the A2 [1] and NA62 [46] Collaborations and the calculations with Padé approximants [49] and the dispersive analysis (DA) from Ref. [9, 10]. The error bars plotted on all data points are based on the errors obtained in the fits to the  $m(e^+e^-\gamma)$  experimental spectra, which are mostly determined by the experimental statistics. In order to facilitate a comparison with the present work, the data points shown for the previous A2 measurement [1] represent the fit results with the smallest  $\delta N(\pi^0 \rightarrow e^+e^-\gamma)/N(\pi^0 \rightarrow e^+e^-\gamma)$ , rather than the results averaged for each bin, with the systematic uncertainties added. In this way, a better view of the improvement reached by the A2 Collaboration, due to the increase in the experimental statistics, is presented. The error bars of the NA62 data points are of the same order of magnitude because their  $m(e^+e^-)$  bins were chosen in such a way to have similar experimental statistics in each bin. The magnitude of their error bars are typically larger than those from the present work over most of the entire range of  $m(e^+e^-)$  masses. A fit to the data points from the present work with Eq.(2) is shown by a solid blue line. The magnitude of the fit parameter  $p_0$  represents the slope parameter  $a_\pi = 0.0315 \pm 0.0026$ , with its uncertainty being close to 8%. The magnitude of  $\chi^2/\text{ndf} = 18.03/21$  from the fit indicates that the scattering of the experimental data points with respect to the fit function is in close agreement with their uncertainties. Because the magnitude of the experimental uncertainties of the  $|F_{\pi^0\gamma}(m_{e^+e^-})|^2$  data points changes significantly with increasing  $m(e^+e^-)$ , a Q-Q test was made for the data-point residuals, which were obtained as the difference between the experimental  $|F_{\pi^0\gamma}(m_{e^+e^-})|^2$  values and the fit function, divided by the corresponding experimental uncertainties. As shown in Fig. 9, the fit residuals plotted versus a normal distribution for the number of experimental data points are distributed closely to the expected linear dependence, depicted by a dashed line.

It was also checked that the inclusion of an additional normalization parameter in the fit function gives a value  $0.9999 \pm 0.0006$  close to unity, proving that it could be neglected for extracting the slope parameter  $a_\pi$ , to avoid enlarging the  $a_\pi$  uncertainty because of the correlation between the two parameters. As also shown in Fig. 8, the slope-parameter fit to the present data points agrees very closely with the latest DA calculation [9, 10] and is also within the error band of the calculation with Padé approximants [49].

As discussed above, the fitting procedure for each individual  $m(e^+e^-)$  bin was repeated multiple times after refilling the  $m(e^+e^-\gamma)$  spectra with different combinations of selection criteria, which improved the signal-to-background ratio, but lost some fraction of the signal events. The main tests were performed for events selected with and without PID  $dE/dx$  cuts, with tightening PID  $dE/dx$  cuts and the kinematic-fit CL, and removing events with higher incident-photon energies to reduce possible background from the reactions  $\gamma p \rightarrow \pi^0 \pi^0 p$  and  $\gamma p \rightarrow \pi^0 \pi^+ n$ . The selection of those  $|F_{\pi^0\gamma}(m_{e^+e^-})|^2$  results for fitting with Eq.(2) was then based on using sim-

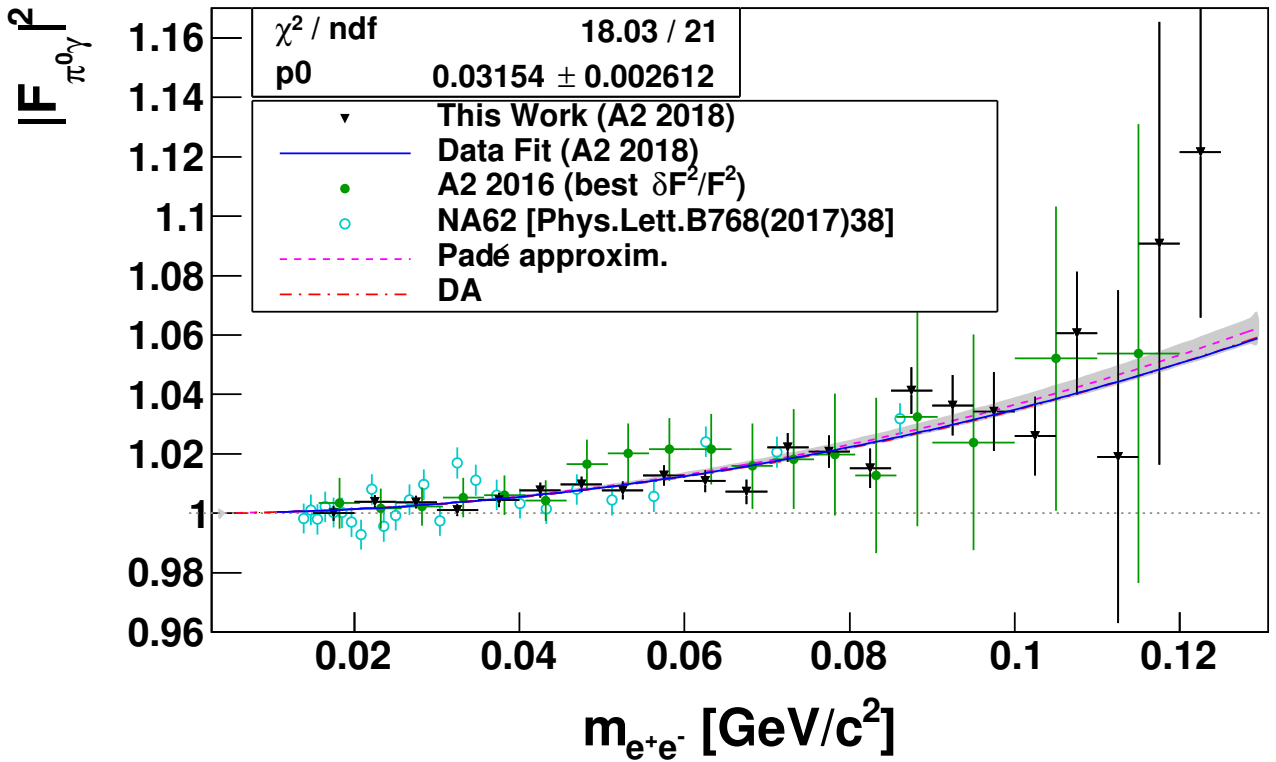


FIG. 8: (Color online)  $|F_{\pi^0\gamma}|^2$  results (black filled triangles) obtained in the present work are fitted with Eq.(2) (shown by the blue line, with  $p_0$  being the fitted slope parameter  $a_\pi$ ) are compared to the data points of the previous measurements by the A2 [1] (green filled circles) and NA62 [46] (cyan circles) Collaborations and to the calculations with Padé approximants [49] (shown by the short-dashed magenta line with an error band) and to the dispersive analysis (DA) from Ref. [9, 10] (long-dashed red line). The DA error band is not shown here because of its smallness. The error bars on all data points are based on the errors obtained in the fits to the  $m(e^+e^-\gamma)$  experimental spectra, which are mostly determined by the experimental statistics.

TABLE I: Results of this work for the  $\pi^0$  TFF,  $|F_{\pi^0\gamma}|^2$ , as a function of the invariant mass  $m(e^+e^-)$  obtained for 22 5-MeV-wide  $m(e^+e^-)$  bins in the invariant-mass range  $15 < m(e^+e^-) < 125$  MeV/ $c^2$ , where the uncertainties are based on the fits to the experimental spectra, reflecting the number of  $\pi^0 \rightarrow e^+e^-\gamma$  decays observed in each bin. The number of significant digits in the listed  $|F_{\pi^0\gamma}|^2$  value was left identical to those used in their fit with the slope parameter. The  $|F_{\pi^0\gamma}|^2$  (LO) results are obtained with radiative corrections including only the LO terms.

$m(e^+e^-)$ [MeV/ $c^2$ ]	$17.5 \pm 2.5$	$22.5 \pm 2.5$	$27.5 \pm 2.5$	$32.5 \pm 2.5$	$37.5 \pm 2.5$
$ F_{\pi^0\gamma} ^2$	$0.99998 \pm 0.00246$	$1.00382 \pm 0.00218$	$1.00375 \pm 0.00217$	$1.00110 \pm 0.00208$	$1.00450 \pm 0.00236$
$ F_{\pi^0\gamma} ^2$ (LO)	$0.99989 \pm 0.00246$	$1.00358 \pm 0.00218$	$1.00335 \pm 0.00217$	$1.00049 \pm 0.00208$	$1.00380 \pm 0.00236$
$m(e^+e^-)$ [MeV/ $c^2$ ]	$42.5 \pm 2.5$	$47.5 \pm 2.5$	$52.5 \pm 2.5$	$57.5 \pm 2.5$	$62.5 \pm 2.5$
$ F_{\pi^0\gamma} ^2$	$1.00779 \pm 0.00252$	$1.00973 \pm 0.00262$	$1.00772 \pm 0.00303$	$1.01272 \pm 0.00342$	$1.01086 \pm 0.00367$
$ F_{\pi^0\gamma} ^2$ (LO)	$1.00686 \pm 0.00252$	$1.00848 \pm 0.00262$	$1.00617 \pm 0.00303$	$1.01079 \pm 0.00341$	$1.00853 \pm 0.00366$
$m(e^+e^-)$ [MeV/ $c^2$ ]	$67.5 \pm 2.5$	$72.5 \pm 2.5$	$77.5 \pm 2.5$	$82.5 \pm 2.5$	$87.5 \pm 2.5$
$ F_{\pi^0\gamma} ^2$	$1.00721 \pm 0.00421$	$1.02222 \pm 0.00486$	$1.02069 \pm 0.00543$	$1.01511 \pm 0.00659$	$1.04125 \pm 0.00785$
$ F_{\pi^0\gamma} ^2$ (LO)	$1.00445 \pm 0.00420$	$1.01889 \pm 0.00484$	$1.01685 \pm 0.00541$	$1.01065 \pm 0.00656$	$1.03613 \pm 0.00781$
$m(e^+e^-)$ [MeV/ $c^2$ ]	$92.5 \pm 2.5$	$97.5 \pm 2.5$	$102.5 \pm 2.5$	$107.5 \pm 2.5$	$112.5 \pm 2.5$
$ F_{\pi^0\gamma} ^2$	$1.03634 \pm 0.01011$	$1.03428 \pm 0.01322$	$1.02597 \pm 0.01327$	$1.06060 \pm 0.02074$	$1.01904 \pm 0.05599$
$ F_{\pi^0\gamma} ^2$ (LO)	$1.03064 \pm 0.01005$	$1.02967 \pm 0.01316$	$1.02050 \pm 0.01320$	$1.05562 \pm 0.02064$	$1.00732 \pm 0.05535$
$m(e^+e^-)$ [MeV/ $c^2$ ]	$117.5 \pm 2.5$	$122.5 \pm 2.5$			
$ F_{\pi^0\gamma} ^2$	$1.09086 \pm 0.07455$	$1.12150 \pm 0.05574$			
$ F_{\pi^0\gamma} ^2$ (LO)	$1.08401 \pm 0.07408$	$1.11955 \pm 0.05564$			

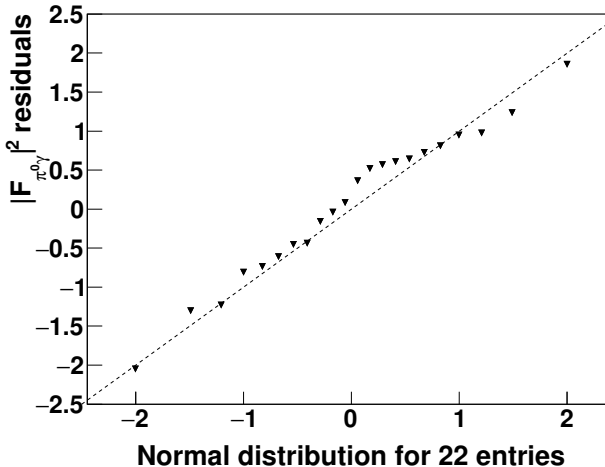


FIG. 9: Q-Q test checking whether the  $|F_{\pi^0\gamma}(m_{e^+e^-})|^2$  residuals follow the normal distribution.

ilar sets of selection criteria for each test to see changes in the magnitude obtained for the slope parameter. The root mean square of all the test values obtained for  $a_\pi$  was taken as its systematic uncertainty, resulting in the final value of this work

$$a_\pi = 0.0315 \pm 0.0026_{\text{stat}} \pm 0.0010_{\text{syst}}. \quad (6)$$

This result is in good agreement within the experimental uncertainties with the most recent measurements by the A2 Collaboration,  $a_\pi = 0.030 \pm 0.010_{\text{tot}}$ , and by the NA62 Collaboration,  $a_\pi = 0.0368 \pm 0.0051_{\text{stat}} \pm 0.0025_{\text{syst}} = 0.0368 \pm 0.0057_{\text{tot}}$ . A similar agreement is observed with the calculations from Ref. [49],  $a_\pi = 0.0324 \pm 0.0012_{\text{stat}} \pm 0.0019_{\text{syst}}$ , and Ref. [9, 10],  $a_\pi = 0.0315 \pm 0.0009$ ; although the uncertainty obtained for  $a_\pi$  in the present measurement is still larger than in those calculations. At the same time, the uncertainty in the current RPP value,  $a_\pi = 0.0332 \pm 0.0029$  [42], is slightly larger than the one in the present measurement. In addition, the statistical accuracy of the present  $|F_{\pi^0\gamma}(m_{e^+e^-})|^2$  data points is still insufficient to fit them with Eq.(5), resulting in a strong correlation between the slope parameter  $a_\pi$  and the curvature parameter  $b_\pi$ .

The numerical values obtained for the individual  $|F_{\pi^0\gamma}(m_{e^+e^-})|^2$  results in each  $m(e^+e^-)$  bin are listed in Table I in order to facilitate their comparison with existing data and theoretical calculations and for using in model-independent fits. The sensitivity of the present  $|F_{\pi^0\gamma}(m_{e^+e^-})|^2$  results and the measured value for the slope parameter to the magnitude of radiative corrections was tested by removing their three NLO terms, assuming that the LO term is well known and that introducing additionally NNLO terms could change the results of this work. The results of this test were listed in Table I as  $|F_{\pi^0\gamma}(m_{e^+e^-})|^2$  (LO). Because the change in the experimental acceptance after removing only NLO terms is quite small, the  $|F_{\pi^0\gamma}(m_{e^+e^-})|^2$  (LO) data points could

be used in case there will be an update of radiative corrections for their NLO and NNLO terms. Fitting the  $|F_{\pi^0\gamma}(m_{e^+e^-})|^2$  (LO) data points with Eq.(2) results in  $a_\pi(\text{LO}) = 0.0262 \pm 0.0026$ , which is significantly lower than the actual  $a_\pi$  obtained in this work, confirming a strong sensitivity of the results obtained in this work to the magnitude of radiative corrections.

## V. SUMMARY AND CONCLUSIONS

The Dalitz decay  $\pi^0 \rightarrow e^+e^-\gamma$  has been measured with the highest up-to-date statistical accuracy in the  $\gamma p \rightarrow \pi^0 p$  reaction with the A2 tagged-photon facility at the Mainz Microtron, MAMI. The value obtained for the slope parameter of the  $\pi^0$  e/m TFF,  $a_\pi = 0.0315 \pm 0.0026_{\text{stat}} \pm 0.0010_{\text{syst}}$ , agrees within the uncertainties with the existing measurements of this decay and with the recent theoretical calculations. The uncertainty obtained in the value of  $a_\pi$  is lower than in previous results based on the  $\pi^0 \rightarrow e^+e^-\gamma$  decay. The results of this work also include  $|F_{\pi^0\gamma}(m_{ee})|^2$  data points and their uncertainties, allowing comparison of the present data with previous measurements and theoretical calculations or using these data in model-independent fits. It is expected that adding the present value for  $a_\pi$  in its RPP average will result in further decrease of the uncertainty in the RPP average value. However, it will still be insufficient for any significant constraining the calculations used to estimate  $(g-2)_\mu$  contributions from the pion-pole term  $a_\mu^{\pi^0}$  to the HLbL scattering and the  $\pi^0\gamma$  term  $a_\mu^{\pi^0\gamma}$  to the HVP correction, which are mostly determined by the data-driven calculations of the  $\pi^0$  electromagnetic transition form factor  $a_\pi$  [9, 10], having significantly smaller uncertainties.

## Acknowledgments

The authors wish to acknowledge the excellent support of the accelerator group and operators of MAMI. We would like to stress the importance of involvement of Tomáš Husek in the present and previous A2 analysis [1] in providing a program to calculate radiative corrections and helpful discussion of the possible impact of those corrections on the magnitude of the slope parameter extracted from the experimental data. We would like to thank Bastian Kubis and Pere Masjuan for useful discussions and continuous interest in the paper. This work was supported by the Deutsche Forschungsgemeinschaft (DFG, German Research Foundation) within the Research Unit “Photon-photon interactions in the Standard Model and beyond” (Project No.458854507 - FOR 5327), the European Community-Research Infrastructure Activity under the FP6 “Structuring the European Research Area” program (Hadron Physics, Contract No. RII3-CT-2004-506078), Schweizerischer Nationalfonds (Contract Nos. 200020-156983, 132799, 121781, 117601, 113511), the U.K. Science and

Technology Facilities Council (STFC 57071/1, 50727/1, ST/Y000285/1), the U.S. Department of Energy (Offices of Science and Nuclear Physics, Award Nos. DE-FG02-99-ER41110, DE-FG02-88ER40415, DE-FG02-01-ER41194) and National Science Foundation (Grant Nos. PHY-1039130, PHY-1714833, PHY-2012940, PHY-

2310026, IIA-1358175), NSERC of Canada (Grant Nos. 371543-2012, SAPPJ-2015-00023), and INFN (Italy). We thank the undergraduate students of Mount Allison University and The George Washington University for their assistance.

---

[1] P. Adlarson *et al.*, Phys. Rev. C **95** (2017)2, 025202.

[2] A. Nyffeler, Phys. Rev. D **94**, 053006 (2016).

[3] T. Aoyama *et al.*, Phys. Rep. **887**, 1 (2020).

[4] R. Aliberti *et al.*, Phys. Rep. **1143**, 1 (2025).

[5] G. Colangelo, M. Hoferichter, B. Kubis, M. Procura, and P. Stoffer, Phys. Lett. B **738**, 6 (2014).

[6] G. Colangelo, M. Hoferichter, M. Procura, and P. Stoffer, J. High Energy Phys. **09**, 074 (2015).

[7] P. Masjuan and P. Sánchez-Puertas, Phys. Rev. D **95**, 054026 (2017).

[8] G. Colangelo, M. Hoferichter, M. Procura, and P. Stoffer, J. High Energy Phys. **04**, 161 (2017).

[9] M. Hoferichter, B.-L. Hoid, B. Kubis, S. Leupold, and S. P. Schneider, Phys. Rev. Lett. **121**, 112002 (2018).

[10] M. Hoferichter, B.-L. Hoid, B. Kubis, S. Leupold, and S. P. Schneider, J. High Energy Phys. **10**, 141 (2018).

[11] G. Eichmann, C. S. Fischer, E. Weil, and R. Williams, Phys. Lett. B **797**, 134855 (2019), [Erratum: Phys. Lett. B **799**, 135029 (2019)].

[12] J. Bijnens, N. Hermansson-Truedsson, and A. Rodríguez-Sánchez, Phys. Lett. B **798**, 134994 (2019).

[13] J. Leutgeb and A. Rebhan, Phys. Rev. D **101**, 114015 (2020).

[14] L. Cappiello, O. Catà, G. D'Ambrosio, D. Greynat, and A. Iyer, Phys. Rev. D **102**, 016009 (2020).

[15] P. Masjuan, P. Roig, and P. Sánchez-Puertas, J. Phys. G **49**, 015002 (2022).

[16] J. Bijnens, N. Hermansson-Truedsson, L. Laub, and A. Rodríguez-Sánchez, J. High Energy Phys. **10**, 203 (2020).

[17] J. Bijnens, N. Hermansson-Truedsson, L. Laub, and A. Rodríguez-Sánchez, J. High Energy Phys. **4**, 240 (2021).

[18] I. Danilkin, M. Hoferichter, and P. Stoffer, Phys. Lett. B **820**, 136502 (2021).

[19] D. Stamen, D. Hariharan, M. Hoferichter, B. Kubis, and P. Stoffer, Eur. Phys. J. C **82**, 432 (2022).

[20] J. Leutgeb, J. Mager, and A. Rebhan, Phys. Rev. D **107**, 054021 (2023).

[21] M. Hoferichter, B. Kubis, and M. Zanke, J. High Energy Phys. **8**, 209 (2023).

[22] M. Hoferichter, P. Stoffer, and M. Zillinger, J. High Energy Phys. **4**, 092 (2024).

[23] E. J. Estrada, S. González-Solís, A. Guevara, and P. Roig, J. High Energy Phys. **12**, 203 (2024).

[24] J. Lüdtke, M. Procura, and P. Stoffer, J. High Energy Phys. **4**, 130 (2025).

[25] O. Deineka, I. Danilkin, and M. Vanderhaeghen, Phys. Rev. D **111**, 034009 (2025).

[26] G. Eichmann, C. S. Fischer, T. Haeuser, and O. Regenfelder, Eur. Phys. J. C **85**, 445 (2025).

[27] J. Bijnens, N. Hermansson-Truedsson, and A. Rodríguez-Sánchez, J. High Energy Phys. **3**, 094 (2025).

[28] M. Hoferichter, P. Stoffer, and M. Zillinger, J. High Energy Phys. **2**, 121 (2025).

[29] S. Holz, M. Hoferichter, B.-L. Hoid, and B. Kubis, J. High Energy Phys. **4**, 147 (2025).

[30] L. Cappiello, J. Leutgeb, J. Mager, and A. Rebhan, J. High Energy Phys. **7**, 033 (2025).

[31] F. Jegerlehner, Springer Tracts Mod. Phys. **274**, 1 (2017).

[32] M. Davier, A. Hoecker, B. Malaescu, and Z. Zhang, Eur. Phys. J. C **77**, 827 (2017).

[33] A. Keshavarzi, D. Nomura, and T. Teubner, Phys. Rev. D **97**, 114025 (2018).

[34] A. Keshavarzi, D. Nomura, and T. Teubner, Phys. Rev. D **101**, 014029 (2020).

[35] M. Davier, A. Hoecker, B. Malaescu, and Z. Zhang, Eur. Phys. J. C **80**, 241 (2020), [Erratum: Eur. Phys. J. C **80**, 410 (2020)].

[36] B.-L. Hoid, M. Hoferichter, and B. Kubis, Eur. Phys. J. C **80**, 988 (2020).

[37] C. Bouchiat and L. Michel, J. Phys. Radium **22**, 121 (1961).

[38] S. J. Brodsky and E. de Rafael, Phys. Rev. **168** 1620 (1968).

[39] N. M. Kroll and W. Wada, Phys. Rev. **98**, 1355 (1955).

[40] L. G. Landsberg, Phys. Rep. **128**, 301 (1985).

[41] J. J. Sakurai, *Currents and Mesons*, University of Chicago Press, Chicago, USA, 1969.

[42] S. Navas *et al.*, (Particle Data Group), Phys. Rev. D **110**, 030001 (2024).

[43] R. Arnaldi *et al.*, Phys. Lett. B **757**, 47 (2016).

[44] T. Husek, K. Kampf, and J. Novotný, Phys. Rev. D **92**, 054027 (2015).

[45] K. Mikaelian and J. Smith, Phys. Rev. D **5**, 1763 (1972).

[46] C. Lazzeroni *et al.*, Phys. Lett. B **768**, 38 (2017).

[47] K. A. Olive *et al.*, (Particle Data Group), Chin. Phys. C **38**, 090001 (2014).

[48] H. J. Behrend *et al.*, Z. Phys. C **49**, 401 (1991).

[49] P. Masjuan, Phys. Rev. D **86**, 094021 (2012).

[50] J. Gronberg *et al.*, Phys. Rev. D **57**, 33 (1998).

[51] P. del Amo Sanchez *et al.*, Phys. Rev. D **84**, 052001 (2011).

[52] S. Uehara *et al.*, Phys. Rev. D **86**, 092007 (2012).

[53] M. Hoferichter, B. Kubis, S. Leupold, F. Niecknig, and S. P. Schneider, Eur. Phys. J. C **74**, 3180 (2014).

[54] F. Niecknig, B. Kubis, and S. P. Schneider, Eur. Phys. J. C **72**, 2014 (2012).

[55] M. Hoferichter, B. Kubis, and D. Sakkas, Phys. Rev. D **86**, 116009 (2012).

[56] H. Herminghaus *et al.*, IEEE Trans. Nucl. Sci. **30**, 3274 (1983).

[57] K.-H. Kaiser *et al.*, Nucl. Instrum. Methods Phys. Res. A **593**, 159 (2008).

[58] J. C. McGeorge *et al.*, Eur. Phys. J. A **37**, 129 (2008).

[59] E. Mornacchi, Ph.D. Thesis, Johannes Gutenberg-Universität Mainz,

<http://doi.org/10.25358/openscience-6051>.

- [60] A. Starostin *et al.*, Phys. Rev. C **64**, 055205 (2001).
- [61] R. Novotny, IEEE Trans. Nucl. Sci. **38**, 379 (1991).
- [62] A. R. Gabler *et al.*, Nucl. Instrum. Methods Phys. Res. A **346**, 168 (1994).
- [63] S. Prakhov *et al.*, Phys. Rev. C **79**, 035204 (2009).
- [64] E. F. McNicoll *et al.*, Phys. Rev. C **82**, 035208 (2010).
- [65] A. Nikolaev *et al.*, Eur. Phys. J. A **50**, 58 (2014).
- [66] D. Watts, *Proceedings of the 11th International Conference on Calorimetry in Particle Physics*, Perugia, Italy, 2004 (World Scientific, Singapore, 2005), p. 560.
- [67] D. Hornidge *et al.*, Phys. Rev. Lett. **111**, 062004 (2013).
- [68] P. Adlarson *et al.*, Phys. Rev. C **92**, 024617 (2015).